

Research Article

Open Access



One-pot synthesis of N-containing heterocycles from bioethanol via dehydrogenative dual-cross-condensation

Jian Zhang^{1,2}, Lijun Liang¹, Yanru Zhu^{1,2}, Xin Shu¹, Hongyan Song¹, Zhe An^{1,2,*}, Jing He^{1,2}

¹State Key Laboratory of Chemical Resource Engineering, Beijing University of Chemical Technology, Beijing 100029, China.

²State Key Laboratory of Chemical Resource Engineering, Quzhou Institute for Innovation in Resource Chemical Engineering, Quzhou 324000, Zhejiang, China.

*Correspondence to: Prof. Zhe An, State Key Laboratory of Chemical Resource Engineering, Beijing University of Chemical Technology, 15 North Third Ring East Road, Beijing 100029, China. E-mail: anzhe@mail.buct.edu.cn

How to cite this article: Zhang, J.; Liang, L.; Zhu, Y.; Shu, X.; Song, H.; An, Z.; He, J. One-pot synthesis of N-containing heterocycles from bioethanol via dehydrogenative dual-cross-condensation. *Chem. Synth.* **2025**, *5*, 61. <https://dx.doi.org/10.20517/cs.2025.03>

Received: 8 Jan 2025 **First Decision:** 20 Feb 2025 **Revised:** 27 Mar 2025 **Accepted:** 10 Apr 2025 **Published:** 9 Jul 2025

Academic Editor: Aicheng Chen **Copy Editor:** Xing-Yue Zhang **Production Editor:** Xing-Yue Zhang

Abstract

Green synthesis of N-containing heterocycles has drawn increasing attention due to their significant applications in pharmaceuticals, dyes, and materials, while remains a great challenge. Herein, we propose a one-pot synthesis of N-containing heterocycles from bioethanol and amino alcohols via dehydrogenative dual-cross-condensation and secondary-cross-condensation by cascade catalysis. Isolated yields of 93% to pyrrole in reaction of bioethanol with 2-aminoethanol, 95% to N-ethyl-1,2,3,4-tetrahydroquinoline in reaction of bioethanol with 2-aminobenzyl alcohol, and 94% to N-ethyl piperidine in reaction of bioethanol with 3-aminopropanol have been achieved using a Ni catalyst supported Zr-containing layered double oxides without any additives. This work provides not only a green and sustainable method for production of the N-containing heterocycles but also a promising way for the sustainable use of bioethanol and even biomass industry.

Keywords: N-containing heterocycles, bioethanol, green synthesis, cross-condensation, supported Ni catalyst

INTRODUCTION

Given the ongoing energy demand, depletion of fossil-based resources, and environmental concerns, it is



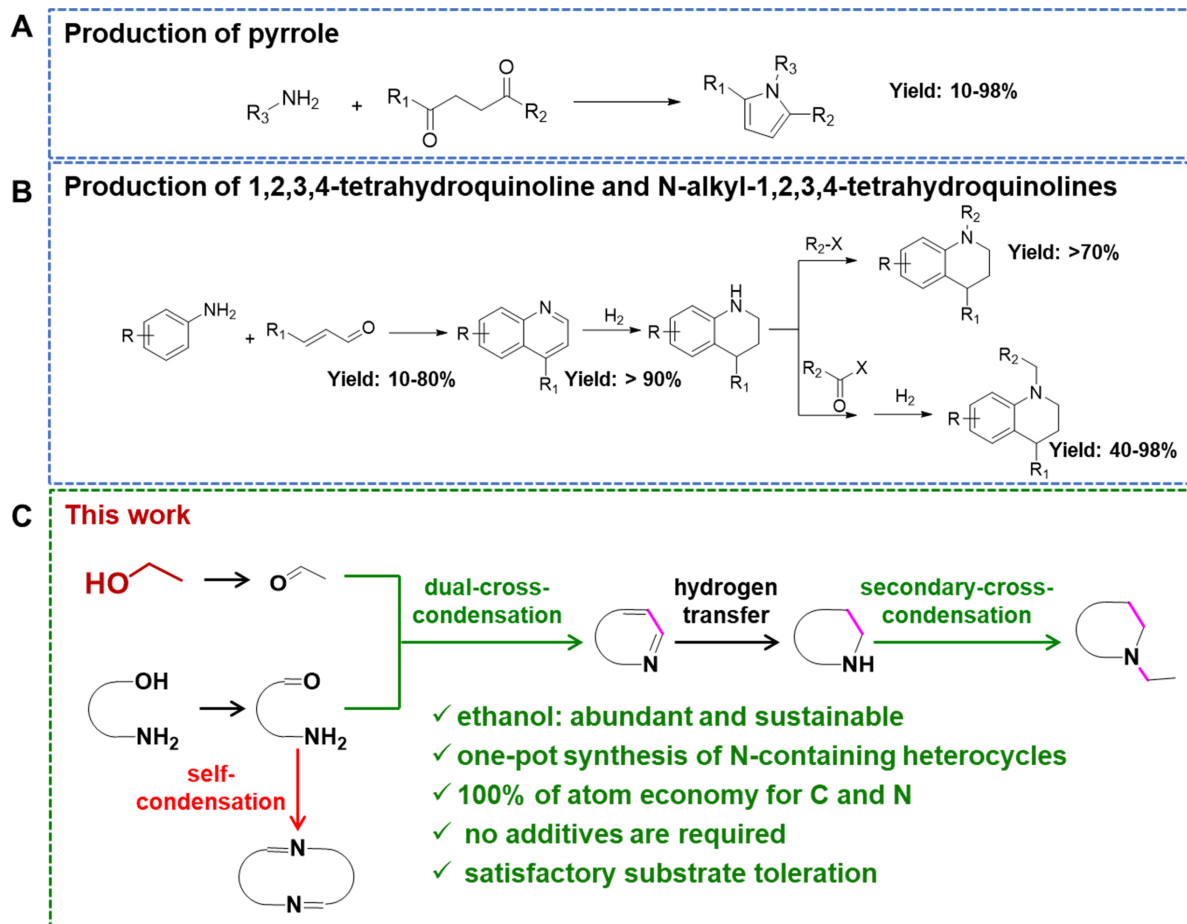
© The Author(s) 2025. **Open Access** This article is licensed under a Creative Commons Attribution 4.0 International License (<https://creativecommons.org/licenses/by/4.0/>), which permits unrestricted use, sharing, adaptation, distribution and reproduction in any medium or format, for any purpose, even commercially, as long as you give appropriate credit to the original author(s) and the source, provide a link to the Creative Commons license, and indicate if changes were made.



increasingly imperative to develop sustainable energy sources. Biomass, as the only renewable carbon resource in nature, has been considered a promising feedstock for the production of value-added fuels and chemicals, serving as a renewable alternative to fossil feedstocks^[1-4]. Bioethanol, one of the initial building blocks produced industrially through biomass fermentation with a global production exceeding 100 billion tons per year^[5-7], has been regarded as one of the most important and representative biomass-derived platform molecules. Converting of bioethanol to value-added chemicals is of great significance for the sustainable development of biomass industry and has drawn rising attention. Recently, ethanol has been applied as a raw material in the synthesis of valued-added hydrocarbons^[8-10], such as butadiene, oxygen-containing chemicals^[9-11], such as higher alcohols (C₄-C₁₂ alcohols) and aromatic alcohols/aldehydes, and N-containing chemicals^[12,13], such as amines.

N-containing chemicals are pivotal bulk and fine chemicals with extensive application in the manufacture of pharmaceuticals, dyes, polymer materials, and agrochemicals^[14-19]. More than 80% of the top 200 pharmaceuticals are N-containing chemicals and the annual global market of N-containing chemicals is more than \$50 billion^[15]. Specifically, nearly 75% of unique small-molecule pharmaceuticals contain a N-containing heterocycle^[16], such as pyrrole, 1,2,3,4-tetrahydroquinoline (THQ), and piperidine. Piperidine and its derivatives have been applied in anticancer (Niraparib^[20]) and antipsychotic (Preclamol^[21]) pharmaceuticals. THQ and its derivatives have been widely applied to synthesize biologically active natural products^[22,23], such as angustureine^[22] and aspernigerin^[23], and synthetic pharmacologically relevant agents^[24-26], including antitumor agents^[27], HIV-1 RT inhibitor^[24], nNOS inhibitors^[25], renin inhibitors^[26]. N-ethyl-THQ (NETHQ) and its derivatives have also been recognized as effective human H₃ receptors^[8] and second near-infrared imaging agents^[28]. In addition, THQ and its derivatives are also widely applied as starting materials to synthesize fine chemicals^[17,29-37]. The conductive polypyrrole derived from polymerization of pyrrole has been widely applied in energy storage and conversion^[38-40], sensors^[40,41], actuators^[38,40], and even water pollution control^[40,42]. Industrially, pyrroles were formed by the reaction of ammonia or primary amine with a 1,4-dicarbonyl compound [Scheme 1A]^[43,44], and THQ and its derivatives were produced via hydrogenation of quinolines^[45] that was prepared via reaction of aniline with α,β -unsaturated aldehyde [Scheme 1B]^[46]. The N-alkyl-THQ compounds are synthesized [Scheme 1B] via the N-alkylation of THQs with alkyl halides^[47] or amidation of THQs with acyl chloride followed by a hydrogenation step^[48], which requires excess amounts of halides and produces a large amount of halogen-containing wastewater. Development of methods for production of N-containing heterocycles in an atom-economical, green, and sustainable fashion is highly desired and has drawn great interest.

During the past decade, combination of acceptorless dehydrogenation of alcohols with cross-condensation has become a powerful tool for the benign construction of pyrroles^[49-51], pyridines^[52-54], benzimidazole^[55], and quinolines^[56-58] from conversion of secondary alcohols with 1,2-amino alcohols, 1,3-amino alcohols or 2-aminobenzyl alcohols on homogeneous Ru, Ir, or Mn complexes. Despite the significant progress achieved, the applicability of the alcohols is limited to the secondary alcohols with excessive indispensable base additives. Undoubtedly, transforming bioethanol to value-added N-containing heterocycles is a preferred protocol due to the following benefits: (1) bioethanol is a nontoxic and easy-to-access feedstock with a production of more than 100 billion tons per year; (2) the production of N-containing heterocycles from bioethanol is a zero-carbon and even negative-carbon way with the sole by-product of water; (3) the production of N-containing heterocycles from bioethanol broadens the downstream chains of bioethanol industry, which is of great significance for the sustainable development of bioethanol and even the biomass industry. However, highly efficient formation of N-containing heterocycles from ethanol presents great challenges: (1) the uphill for ethanol direct dehydrogenation to acetaldehyde ($\Delta G_{298\text{ K}} = 13.1\text{ kcal}\cdot\text{mol}^{-1}$ at 1 atm)^[59] makes ethanol direct dehydrogenation process proceed at a high working temperature, which



Scheme 1. (A) Production methodology for pyrrole and (B) 1,2,3,4-tetrahydroquinoline and N-alkyl-1,2,3,4-tetrahydroquinolines; (C) The proposed reaction pathways for one-pot green and sustainable production of N-containing heterocycles from bioethanol.

could easily cause ethanol dehydration to ethyl ether or ethylene; (2) the dual-cross-condensation and secondary-cross-condensation face competition from the self-condensation between acetaldehyde with ethanol to acetate or diethoxy ethane and between amino-aldehyde itself, resulting in the low selectivity to N-containing heterocycles; (3) the cascade reactions might stop at the intermediates and it is difficult to obtain the targeted N-containing heterocycles.

Here we propose the one-pot green and sustainable production of N-containing heterocycles from bioethanol and amino-alcohols [Scheme 1C]. In our previous work^[60], our group has claimed the first synthesis of THQ and its derivatives from 2-aminobenzyl alcohols and ethanol on a heterogeneous Ni catalyst: the Ni⁰-Ni^{δ+} synergistic catalysis is responsible for alcohol dehydrogenation and hydrogen transfer while the acidic/basic sites for the dual-cross-condensation for the formation of C=C/C=N bond. By engineering the Ni⁰-Ni^{δ+} synergistic catalysis via Ni particle size and post-treatment, isolated yields of 95% to THQ have been achieved. However, the reaction stopped at THQ without achieving the NETHQ. In this work, the influence of acidic/basic sites on the dual-cross-condensation and even secondary-cross-condensation was investigated in detail and the competition between dual-cross-condensation and even secondary-cross-condensation with self-condensation was modulated for the targeted production of the N-containing heterocycles. The ability for both dual-cross-condensation and secondary-cross condensation increases with the acidic sites of the catalyst, resulting in isolated yields of 93% to pyrrole from reaction of

bioethanol with 2-aminoethanol, 95% to NETHQ from reaction of bioethanol with 2-aminobenzyl alcohol, and 94% to N-ethyl piperidine from reaction of bioethanol with 3-aminopropanol on Zr containing layered double oxides supported Ni (Ni-Zr-LDO) via *in-situ* topological transformation of Ni and Zr-containing layered double hydroxides (Ni-Zr-LDHs) without any addition of additives. After simple recovery by centrifugation, the catalyst could be directly reused and no decrease in either activity or selectivity is detected, showing great potential for industrialization. This work undoubtedly provides a green and sustainable method for production of value-added N-containing heterocycles.

EXPERIMENTAL

Chemicals

Ni(NO₃)₂·6H₂O, Al(NO₃)₃·9H₂O, Mg(NO₃)₂·6H₂O, Zn(NO₃)₂·6H₂O, ZrO(NO₃)₂·xH₂O, NaOH, and Na₂CO₃ were purchased from Sinopharm Chemical Reagents Ltd. Anhydrous ethanol, 2-aminobenzyl alcohol, substituted 2-aminobenzyl alcohols, 2-aminobenzaldehyde, acetaldehyde, 2-aminoethanol, and 3-aminopropanol were purchased from Aladdin Reagents Co., Ltd. All chemicals were used directly without subsequent purification.

Preparations

NiMgAl-LDHs, NiZnAl-LDHs, NiAl-LDHs, and NiAlZr-LDHs

The NiAl-LDHs with Ni/Al molar ratio 2/1, NiAlZr-LDHs with Ni/Al/Zr molar ratio 2/0.9/0.1, NiMgAl-LDHs with Ni/Mg/Al molar ratio 0.81/3.0/1, and NiZnAl-LDHs with Ni/Zn/Al molar ratio 0.7/1.5/1, 0.9/2.0/1, and 1.1/2.5/1 in the synthesis mixture were prepared via a nucleation/crystallization separation method^[61]. Typically, 11.632 g (0.04 mmol) of Ni(NO₃)₂·6H₂O, 6.7524 g (0.018 mol) of Al(NO₃)₃·9H₂O, and 0.4625 g (0.002 mol) of ZrO(NO₃)₂·xH₂O were dissolved into 200 mL of deionized water, forming solution A. 4.8 g (0.12 mol) of NaOH and 1.06 g (0.01 mol) of Na₂CO₃ were dissolved into 200 mL of deionized water, forming solution B. Then the solution A and B were simultaneously poured into a colloid mill with a rotating speed of 5,000 rpm. Two minutes later, the resulting slurry was transferred to a sealed bottle and aged in an oven at 80 °C for 24 h. Then the precipitates were filtered, washed thoroughly with deionized water till the filtrate was neutral, and dried overnight at 60 °C, forming NiAlZr-LDHs. Similar procedures were applied to the preparation of NiMgAl-LDHs, NiZnAl-LDHs and NiAl-LDHs.

Ni-NiAl-LDO, Ni-NiAlZr-LDO, Ni-ZnAl-LDO, and Ni-MgAl-LDO

Ni-NiAl-LDO or Ni-NiAlZr-LDO was prepared by calcination of NiAl-LDHs or NiAlZr-LDHs at 400 °C for 1 h under H₂ flow in a tube furnace. Ni-Zn_xAl-LDO was prepared by calcination of NiZn_xAl-LDHs at 500 °C for 1 h under H₂ flow. Ni-MgAl-LDO was prepared by calcination of NiMgAl-LDHs at 700 °C for 1 h under H₂ flow. All the temperature-programmed procedures were from ambient temperature to the desired temperature with a heating rate of 5 °C·min⁻¹. After the thermal treatment, the samples were reserved under Ar for characterizations or sealed with ethanol for catalytic test.

Characterizations

The textural structures were recorded on a Brooker V80 diffractometer using Cu Kα radiator (λ = 0.1541 nm) with a scanning rate of 10°/min. The Ni, Mg, Zn, and Al were quantitatively analyzed on an inductively coupled plasma optical emission spectrometer (Agilent 5900 ICP-OES). Transmission electron microscopy (TEM) and high-resolution TEM (HR-TEM) were taken on a Tecnai G² F30 S-TWIN transmission electron microscope at 300 kV accelerating voltage. Quasi A X-ray photoelectron spectra were carried out on an AXIS SUPRA X-ray photoelectron spectroscopy (XPS) equipped with an Al Kα radiator. To avoid exposure to air, after being cooled in a tube furnace, the samples were transferred into a glovebox under Ar and then to an inert gas conveyor in the glovebox. The samples were then transferred to the analysis chamber of the AXIS SUPRA XPS. C 1s peak at 284.8 eV was used as a calibration peak.

NH₃- and CO₂-temperature-programmed desorption (TPD) profiles were obtained using a Micrometric ChemiSorb 2920 chemisorption instrument with a thermal conductivity detector (TCD). Typically, the Ni-LDO samples (100 mg) were pretreated at 400 °C under H₂/He flow for 0.5 h and then cooled to 50 °C to adsorb NH₃ or CO₂. The TPD profiles were recorded from 50 to 400 °C at a heating rate of 10 °C·min⁻¹. *In-situ* Fourier transform infrared (FT-IR) spectra of pyridine adsorption were recorded on an iS50 FT-IR (NICOLET) spectrometer as the procedures reported in our previous report^[60] (for details see the [Supplementary Materials](#)).

For FT-IR spectra of ethanol adsorption, 15 mg of sample was firstly pressed into a self-supporting wafer and then loaded into the *in-situ* IR cell. After treatment under H₂ (20 mL·min⁻¹) at 350 °C for 1 h, the system was cooled in Ar to 120 °C and the spectrum for background was recorded. Then the ethanol was bubbled into the system until equilibrium was reached, and then the system was purged by Ar until the spectra showed no change. The inlet and outlet valves were turn off and the *in-situ* FT-IR spectra were recorded until the spectra showed no change. Then the system was further purged by Ar and the spectra were recorded. For piperidine adsorption/desorption, the system was first evacuated and the spectrum for background was recorded at 50 °C. The piperidine was bubbled into the system and the spectra were recorded until the spectra showed no change. Then the adsorbed piperidine was purged by Ar at 50, 100, 150, 200, and 250 °C for 5 min and the spectrum was recorded respectively.

Catalytic test

First, 30 mg of catalyst was dispersed in 3 mL of ethanol solution containing 0.5 mmol of 2-aminobenzyl alcohol and sealed in a 25 mL pressure-resistant glass reactor. Then the reactor was heated in oil bath of 120 °C for varied time under magnetic stirring. Similar procedures were used for reaction of piperidine, substituted 2-aminobenzyl alcohols, isopropanol, 2-aminoethanol, or 3-aminopropanol (170 °C, in a polytetrafluoroethylene lined stainless steel reactor) with ethanol. For reaction of 2-aminobenzaldehyde (or 2-aminoethanol) and acetaldehyde, 30 mg of catalyst was dispersed in 3 mL of toluene solution containing 0.5 mmol of 2-aminobenzaldehyde or 2-aminoethanol and 2.0 mmol of acetaldehyde. After the reaction, the reactor was quenched by cool water and the catalyst was removed by centrifugation and the liquid products were quantitatively analyzed by gas chromatography (GC) (Shimadzu, 2014C) equipped with a HP-5 column and purified via silica column chromatography (silica, ethyl acetate/N-hexane = 1:5) for nuclear magnetic resonance (NMR) analysis on a Bruker AV-600 (600 MHz) spectrometer (CDCl₃ as the solvent). The NMR analysis for 2-methyl-1,2,3,4-THQ, N-ethyl-piperidine, and pyrrole was performed on a Bruker AV-400 (400 MHz) spectrometer (CDCl₃ as the solvent).

The spent catalyst was recovered by centrifugation and then thoroughly washed with ethanol. Subsequently, the recovered catalyst was directly applied as catalyst in the reaction of 2-aminoethanol with ethanol.

RESULTS AND DISCUSSION

For topological transformation, NiMgAl-LDHs, NiZn_xAl-LDHs (where x represents Zn/Al molar ratio), NiAl-LDHs, and NiAlZr-LDHs were first prepared [[Supplementary Figure 1](#)] via a nucleation/crystallization separation method^[61]. The (003), (006), (012), (015), (018), (110), and (113) reflections typical of LDH structure are clearly observed [[Supplementary Figure 1](#)]. Calcination of NiMgAl-LDHs at 700 °C for 1 h under H₂ atmosphere [[Supplementary Figure 2a](#)] produced both of MgAl-LDO phase with characteristic reflections around 36.6°, 43.5°, and 63.1° (JCPDS: 45-0946) and metallic Ni phase with reflections at 44.5°, 51.9°, and 76.4° (JCPDS: 04-0850). Similarly, after calcination of NiZnAl-LDHs at 500 °C for 1 h under H₂ atmosphere [[Supplementary Figure 2b-d](#)], besides the diffractions of metallic Ni phase at 44.5°, 51.9° and 76.4°, the (100), (002), (101), (110), and (103) reflections characteristic of ZnAl-LDO are also clearly

observed around 31.7° , 34.4° , 36.2° , 56.5° , and 62.8° (JCPDS: 76-0704). The (111), (200), and (220) reflections characteristic of NiAl-LDO (JCPDS: 71-1179) are clearly observed around 37.2° , 43.3° , and 62.9° in Ni-NiAl-LDO [Supplementary Figure 2e] and Ni-NiAlZr-LDO [Supplementary Figure 2f]. No diffractions of ZrO_2 or Al_2O_3 are detected in each case. In the TEM image for Ni-NiAlZr-LDO [Figure 1A], Ni particles are observed to be well dispersed in a narrow distribution with the maximum particle size at 5.0 nm. Similar Ni particle size is observed on Ni-MgAl-LDO [Supplementary Figure 3A], Ni- Zn_xAl -LDO [Supplementary Figure 3B-D], and Ni-NiAl-LDO [Supplementary Figure 3E]. In each case, Ni nanoparticles are observed to be dispersed with (111) facet exposed [Figure 1B and Supplementary Figure 3].

In our previous report^[60], Ni^0 - $\text{Ni}^{\delta+}$ synergy plays a vital role in ethanol dehydrogenation, thereby promoting dual-cross-condensation. In this work, to exclude the effect of electronic properties of Ni on the reaction, the electronic properties of Ni in each case were also detected via quasi *in-situ* XPS. In the Ni $2p_{3/2}$ XPS spectra, binding energies at 855.70 eV assigned to Ni^0 ^[62-64], at 852.97 eV to $\text{Ni}^{\delta+}$ sites^[62-64], and 852.02 eV to Ni^0 sites^[62-64] are observed on Ni- $\text{Zn}_{1.5}\text{Al}$ -LDO [Supplementary Figure 4a]. The $\text{Ni}^{\delta+}$ sites result from the interaction between Ni particles with the support. The binding energies to Ni^0 sites and $\text{Ni}^{\delta+}$ sites slightly shift to 852.31 and 853.74 eV on Ni-NiAl-LDO [Supplementary Figure 4b] and 852.49 and 853.76 eV on Ni-NiAlZr-LDO [Supplementary Figure 4c]. According to the deconvoluted area, the $\text{Ni}^{\delta+}/\text{Ni}^0$ ratio has been quantified and summarized in Supplementary Table 1. The $\text{Ni}^{\delta+}/\text{Ni}^0$ ratio has been determined to be 0.76-0.78 in each Ni-LDO [Supplementary Table 1], implying that the great differences in the following catalytic performance do not contribute to the electronic properties of Ni.

The CO_2 -TPD was then conducted to determine the basic properties of the prepared Ni-LDO. For each sample, a broad CO_2 desorption is observed between 100 and 400 °C [Supplementary Figure 5], which can be deconvoluted into three contributions at the region with a maximal temperature < 170 °C, 190-270 °C, and > 270 °C. The contributions have been identified^[60] as the adsorption of CO_2 on weak, medium-strong, and strong basic sites. The amount of the basic sites is quantified and summarized in Figure 1C. The total amount of basic sites has been determined to be 0.808, 0.205, 0.288, 0.316, 0.524, and 0.535 $\text{mmol}\cdot\text{g}^{-1}$ on Ni-MgAl-LDO, Ni- $\text{Zn}_{1.5}\text{Al}$ -LDO, Ni- $\text{Zn}_{2.0}\text{Al}$ -LDO, Ni- $\text{Zn}_{2.5}\text{Al}$ -LDO, Ni-NiAl-LDO, and Ni-NiAlZr-LDO [Figure 1C], respectively.

The acidic properties of the Ni-LDO were characterized via *in-situ* FT-IR spectra of pyridine adsorption. In the *in-situ* FT-IR spectra of pyridine adsorption [Supplementary Figure 6], a band at $1,457\text{ cm}^{-1}$ is clearly observed while no band is present at $1,540\text{ cm}^{-1}$, indicating that only Lewis (L) acidic sites are detected in each sample. The amount of acidic sites determined on Ni-MgAl-LDO, Ni- $\text{Zn}_{1.5}\text{Al}$ -LDO, Ni- $\text{Zn}_{2.0}\text{Al}$ -LDO, Ni- $\text{Zn}_{2.5}\text{Al}$ -LDO, Ni-NiAl-LDO, and Ni-NiAlZr-LDO are 0.012, 0.030, 0.037, 0.051, 0.080, and 0.121 $\text{mmol}\cdot\text{g}^{-1}$ [Figure 1C], respectively. The NH_3 -TPD has also been applied to identify the strength of the acidic sites. For Ni-NiAl-LDO [Figure 1D], a broad NH_3 desorption is observed between 100 and 420 °C, which can be deconvoluted into three contributions at the region with a maximal temperature of 105, 163, and 215 °C. The contributions have been identified as the adsorption of NH_3 on weak, medium-strong, and strong acidic sites. Compared to the Ni-NiAl-LDO, a new NH_3 desorption peak at 307 °C is visibly observed on Ni-NiAlZr-LDO [Figure 1D], indicating that a stronger L acidic site was introduced with the incorporation of Zr species. These results demonstrate that the Zr species not only increase the amount of acidic sites but also introduce strong acidic sites.

To correlate the selectivity to dual-cross-condensation with the acidic-basic sites [Supplementary Table 2], the Ni-LDO was then applied as catalyst in the reaction of 2-aminobenzaldehyde and acetaldehyde, as given

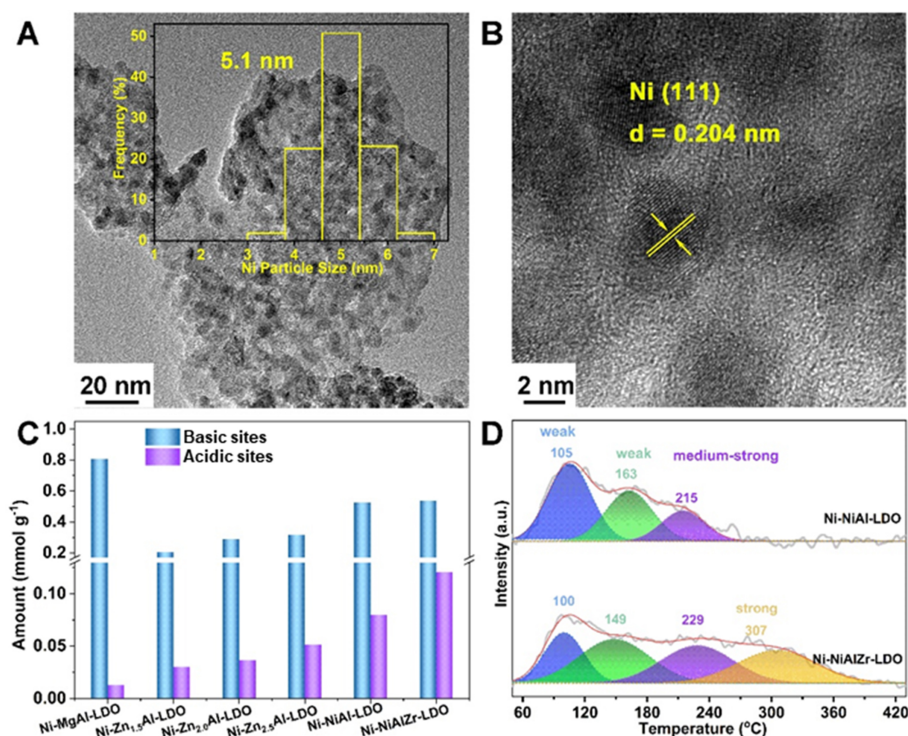
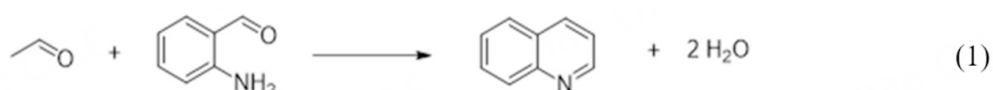


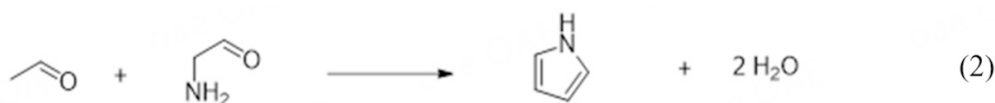
Figure 1. (A) TEM and (B) HRTEM image of Ni-NiAlZr-LDO. Insertion in (A) is the histogram of Ni particle distribution; (C) The basic and acidic properties of the Ni-LDO; (D) NH₃-TPD profiles of Ni-NiAlZr-LDO and Ni-NiAl-LDO. TEM: Transmission electron microscopy; HRTEM: high-resolution TEM; LDO: layered double oxides; TPD: temperature-programmed desorption.

by:



A selectivity of 67% to quinoline, the dual-cross-condensation product, is obtained on Ni-Zn_{1.5}Al-LDO in 2 h. The selectivity to dual-cross-condensation increases with increasing both the acidic and basic sites. On Ni-NiAlZr-LDO with similar basic sites while more acidic sites than Ni-NiAl-LDO, a selectivity of up to 99% to the dual-cross-condensation is obtained, much higher than that on Ni-NiAl-LDO, indicative of the promotion of acidic sites on the dual-cross-condensation. Then correlation between the selectivity to the dual-cross-condensation and the acidic sites was plotted and it has been found that the selectivity to the dual-cross-condensation linearly increases with acidic sites [Figure 2A], further confirming that more acidic sites facilitate the dual-cross-condensation.

The Ni-LDO was also applied as catalyst in the reaction of 2-aminoethanol with acetaldehyde. As seen by monitoring the product composition in the reaction, the fraction of 2-aminoethanol decreases and pyrrole, the dual-cross-condensation product between acetaldehyde and 2-amino acetaldehyde increases over time [Figure 2B], as given in:



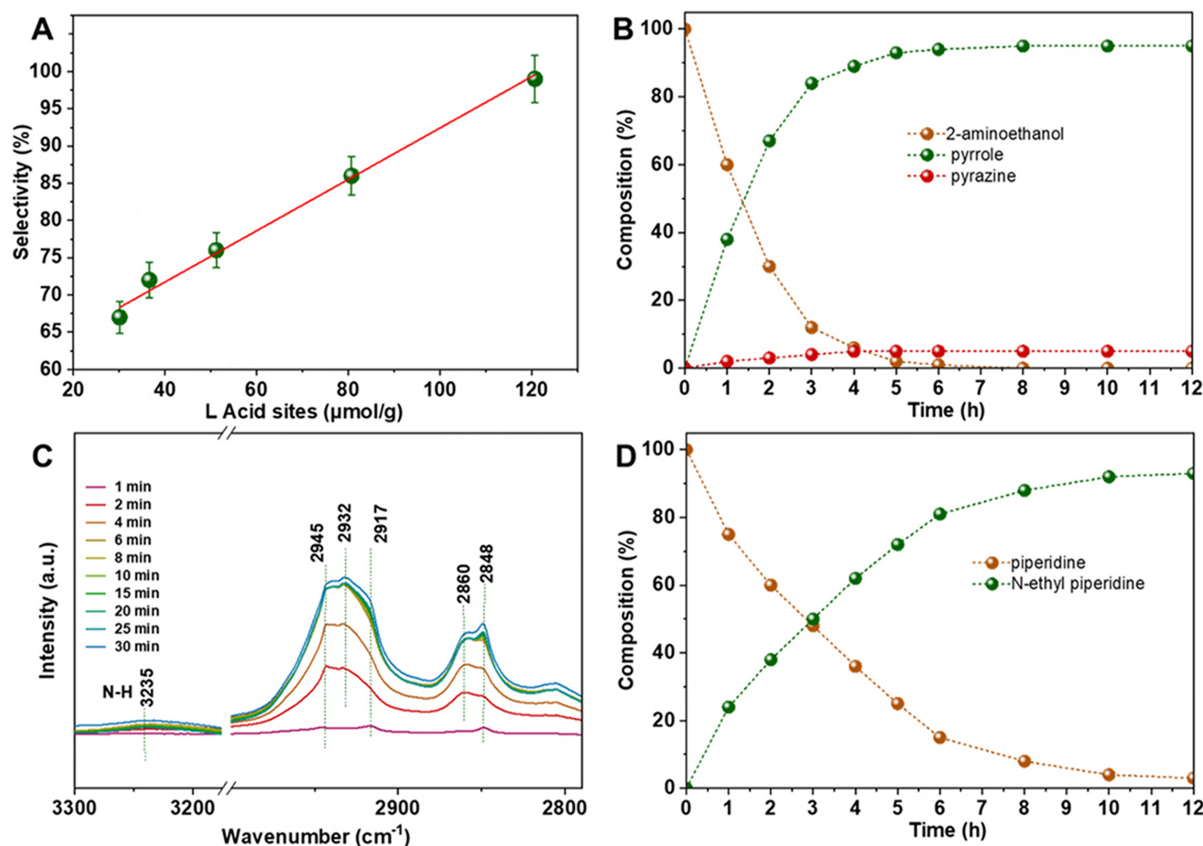


Figure 2. (A) Correlation of the selectivity to dual-cross-condensation with L acidic sites in reaction of 2-aminobenzaldehyde and acetaldehyde; (B) Time course in the reaction between 2-aminoethanol with acetaldehyde on Ni-NiAlZr-LDO at 120 °C under ambient atmosphere; (C) *In-situ* FT-IR of piperidine adsorption on Ni-NiAlZr-LDO at 50 °C; (D) Time course based on piperidine conversion in the reaction between piperidine with ethanol on Ni-NiAlZr-LDO at 120 °C under ambient atmosphere. LDO: Layered double oxides; FT-IR: Fourier transform infrared.

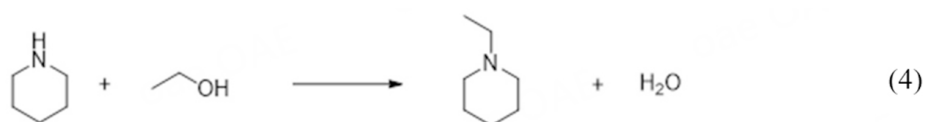
Only trace of pyrazine - the self-condensation product between 2-amino acetaldehyde - is detected, demonstrating the excellent dual-cross-condensation ability on Ni-NiAlZr-LDO, as expressed in:



However, on Ni-NiAl-LDO [Supplementary Figure 7] the pyrazine domains in the products further confirm that the introduction of Zr promotes the dual-cross-condensation. It is noted that no 2-amino acetaldehyde is detected on either Ni-NiAlZr-LDO or Ni-NiAl-LDO, demonstrating the rapid condensation between 2-amino acetaldehyde with acetaldehyde or itself.

In-situ FT-IR spectra using piperidine as the probe molecule were recorded to determine the role of strong L acidic sites on the secondary-cross-condensation. On Ni-NiAlZr-LDO [Figure 2C], the bands at 2,945, 2,917, and 2,848 cm⁻¹ to the stretching mode of C-H bond^[65,66] while no band at 3,235 cm⁻¹ to the stretching mode of N-H bond^[67] are observed under low piperidine coverage (1 min of adsorption), indicative of the dissociation of N-H bond under low piperidine coverage. Increasing adsorption time, new bands at 2,932 and 2,860 cm⁻¹ to C-H bond^[65,66] and at 3,235 cm⁻¹ to N-H bond are detected [Figure 2C], demonstrating the

non-dissociative adsorption of N–H bond under high piperidine coverage. For comparison, only bands at 2,932, 2,860, and 3,235 cm^{-1} to the non-dissociative adsorption of N–H bond are observed on Ni–NiAl–LDO [Supplementary Figure 8], demonstrating that the strong L acidic sites derived from Zr species facilitate the adsorption of piperidine via the interaction between the strong L acidic sites and the lone-pair electrons in N, which facilitates the deprotonation by the basic sites, forming dissociative adsorption of N–H bond. Then, the FT-IR spectra of piperidine desorption were recorded at varied temperatures. Increasing desorption temperature, the bands for non-dissociative adsorption of N–H bond rapidly decrease on Ni–NiAlZr–LDO [Supplementary Figure 9], clearly indicative of the weak adsorption of non-dissociative adsorption of N–H bond. The band at 2,945 cm^{-1} blue shifts to 2,951 cm^{-1} and then slowly declines [Supplementary Figure 9]. On Ni–NiAl–LDO, the band for non-dissociative adsorption of N–H bond rapidly decreases and vanishes at 200 $^{\circ}\text{C}$ [Supplementary Figure 10], further confirming the Zr species on Ni–NiAlZr–LDO provide strong adsorption sites for dissociative adsorption of N–H bond in piperidine. The Ni–NiAlZr–LDO and Ni–NiAl–LDO were then applied as catalysts in the reaction of piperidine with ethanol, as expressed in:



The fraction of piperidine clearly decreases while that of N-ethyl piperidine increases on Ni–NiAlZr–LDO [Figure 2D], indicating that the piperidine converts to N-ethyl piperidine. However, no piperidine conversion is detected on Ni–NiAl–LDO [Supplementary Figure 11]. The FT-IR spectra of the piperidine adsorption/desorption combined with the reaction results clearly demonstrate the strong L acidic sites introduced by Zr species facilitate the dissociation of N–H bond in piperidine, which provides an opportunity for the further cross-condensation between aldehyde and $\text{N}^{\delta-}$ in the piperidine to afford N-ethyl piperidine.

The *in-situ* FT-IR spectra of ethanol adsorption/desorption were recorded to determine the role of the acid-base sites in ethanol dehydrogenation. On Ni–NiAlZr–LDO [Figure 3A], the ethanol adsorption at 120 $^{\circ}\text{C}$ gave absorption bands at 1,576, 1,446, 1,419, 1,378, 1,103, 1,072, and 1,056 cm^{-1} . According to a previous report^[60,68–70], the bands at 1,446 and 1,378 cm^{-1} can be assigned to the modes of CH_2 and CH_3 in adsorbed ethoxide; the band at 1,103 cm^{-1} can be assigned to the stretching mode of C–O bond in on-top ethoxy group; the band at 1,056 cm^{-1} can be assigned to the stretching mode of C–O bond in bridging ethoxide species; the band at 1,072 cm^{-1} can be assigned to the stretching mode of C–O bond in on-top ethoxy group on $\text{Ni}^{\delta+}$ sites; the bands at 1,576 and 1,419 cm^{-1} can be assigned to the ν_s and ν_{as} modes of OCO in adsorbed acetate species. The adsorbed acetate species results from the cleavage of the α -C–H bond in the ethoxy group (generating acetaldehyde) and is followed by reacting with oxygen on the support surface, which creates oxygen vacancies on the support surface. With prolonging the reaction time, the intensity of the bands to acetate peak at 1,576 and 1,419 cm^{-1} increases, while that for the stretching mode of C–O bond in ethoxy species decreases [Figure 3A], demonstrating the process of dehydrogenation of ethoxide to acetaldehyde. Simultaneously, a new band at 1,042 cm^{-1} , which is assigned to the bridging ethoxide on oxygen-defective NiAlZr–LDO, is observed with increasing time [Figure 3A], well accounting for the formation of acetate species. On Ni–ZnAl–LDO [Supplementary Figure 12], similar results are observed to that on Ni–NiAlZr–LDO, except the slower increases in the bands to acetate, slower decrease in the bands for stretching mode of C–O bond in ethoxy species, and the absence of the band at 1,042 cm^{-1} , indicative of the weaker dehydrogenation on Ni–ZnAl–LDO than that on Ni–NiAlZr–LDO. On Ni–NiAl–LDO [Supplementary Figure 13], similar results are observed to that on Ni–NiAlZr–LDO, except the slower increases in the bands to acetate. However, on Ni–MgAl–LDO [Supplementary Figure 14], only bands to on-

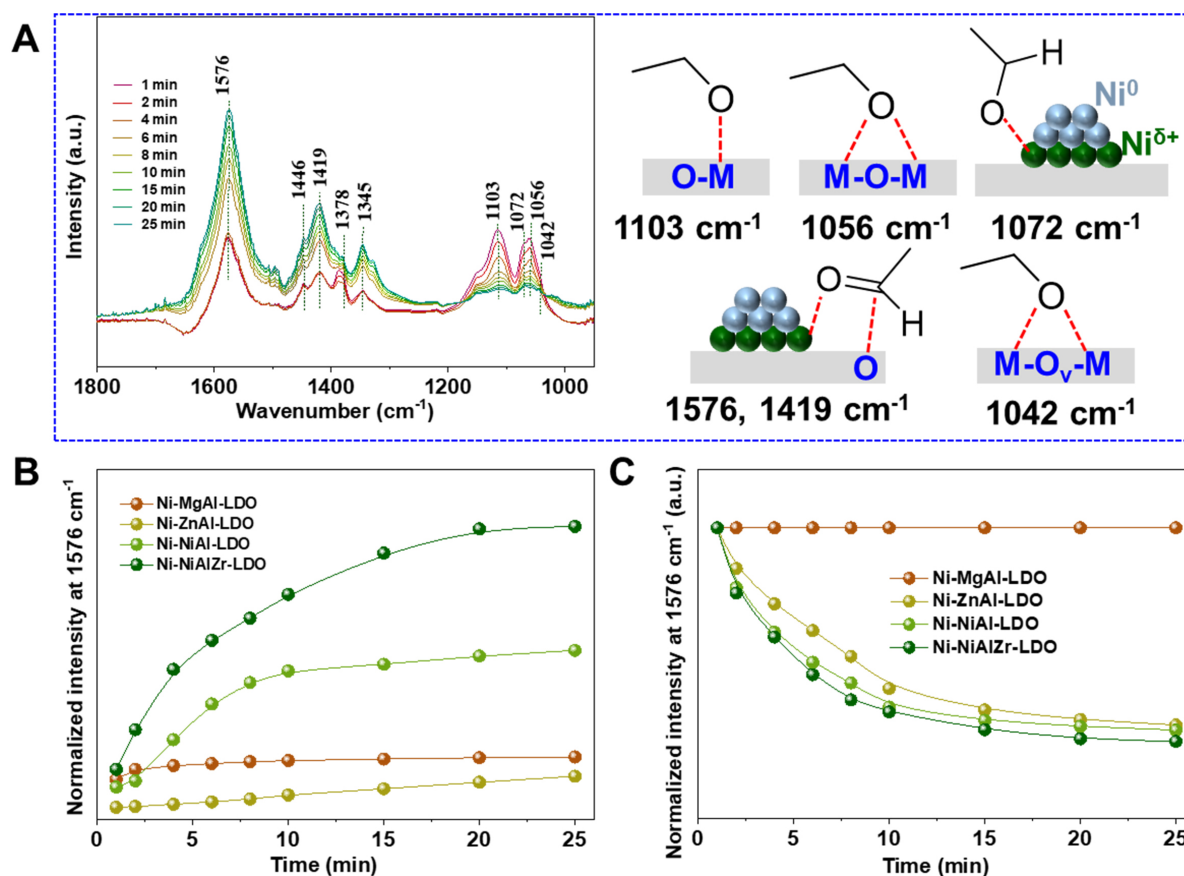
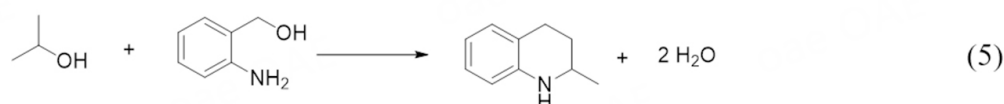


Figure 3. (A) *In-situ* FT-IR spectra of ethanol adsorption on Ni-NiAlZr-LDO at 120 °C under ambient atmosphere; (B) Normalized intensity of the band at 1,576 cm^{-1} as a function of adsorption time ethanol adsorption on varied Ni-LDO at 120 °C; (C) Normalized intensity of the band at 1,576 cm^{-1} as a function of desorption time detected in ethanol desorption on varied Ni-LDO at 120 °C. FT-IR: Fourier transform infrared; LDO: layered double oxides.

top ethoxy at 1,119 cm^{-1} , to the modes of CH_2 and CH_3 in adsorbed ethoxide at 1,457 and 1,389 cm^{-1} , and to adsorbed acetate at 1,576 and 1,436 cm^{-1} are observed while no bridging ethoxy species at 1,056 cm^{-1} and band at 1,072 cm^{-1} are observed. The process of dehydrogenation of ethoxide to acetate is also detected on Ni-MgAl-LDO. To compare the ethanol dehydrogenation ability, the intensity of the band at 1,576 cm^{-1} is normalized and shown in Figure 3B. The higher normalized intensity of the band at 1,576 cm^{-1} on Ni-NiAlZr-LDO demonstrates the higher ethanol dehydrogenation on Ni-NiAlZr-LDO [Figure 3B]. It is noteworthy that no clear increase in the normalized intensity of the band at 1,576 cm^{-1} is detected after 2 min of adsorption on Ni-MgAl-LDO [Figure 3B and Supplementary Figure 14], implying the rapid deactivation of Ni-MgAl-LDO during ethanol adsorption. Then, the system was further purged by Ar, and obvious decreases in intensity of the bands for each intermediate are observed on Ni-NiAlZr-LDO [Supplementary Figure 15], Ni-ZnAl-LDO [Supplementary Figure 16], and Ni-NiAl-LDO [Supplementary Figure 17] while no clear desorption on Ni-MgAl-LDO [Supplementary Figure 18]. Then the intensity for the band at 1,576 cm^{-1} was plotted as a function of desorption time [Figure 3C]. Increasing the acidic sites clearly favors the rapid desorption of the ethanol adsorption intermediates, avoiding the rapid deactivation of catalyst. These results demonstrate the acidic-basic sites play a vital role not only in ethanol dehydrogenation but also in desorption of the intermediates.

Then, the Ni-LDO was applied as catalyst in the reaction of 2-aminobenzyl alcohol with bioethanol at 120 °C under ambient atmosphere. As seen by monitoring the product composition in the reaction, the fraction of 2-aminobenzyl alcohol decreases and that of 2-amino benzaldehyde and THQ increases firstly and then drops over time on Ni-NiAlZr-LDO [Figure 4A]. Simultaneously, the fraction of NETHQ increases over time. Only trace of quinoline is detected, demonstrating the excellent hydrogen transfer ability. These results indicate that the 2-aminobenzaldehyde and THQ are the key intermediates for production of NETHQ on Ni-NiAlZr-LDO [Figure 4A]: 2-aminobenzyl alcohol firstly was converted to 2-amino benzaldehyde, then to THQ, and finally the generated THQ further converts to NETHQ on Ni-NiAlZr-LDO [Supplementary Figure 19]. No NETHQ is afforded on Ni-LDO without the introduction of Zr [Supplementary Figures 20-22], even though increasing the amount of L acidic sites facilitates the dual-cross-condensation ability and promotes the production of THQ [Figure 4B], indicative of the key role of Zr species in the secondary-cross-condensation. Not surprisingly, deactivation is detected after 6 h of reaction on Ni-MgAl-LDO [Supplementary Figure 22], which is consistent with the *in-situ* FT-IR results.

With the optimized reaction conditions, we then examined the generality of this Ni-NiAlZr-LDO catalyzed protocol for N-containing heterocycles. First, the reactions of 2-aminobenzyl alcohol with substituents in 4-position were examined on Ni-NiAlZr-LDO at 120 °C [Figure 4C]. The phenyl, methoxy, methyl formate, and trifluoromethyl substituents on the benzene ring of 2-aminobenzyl alcohol are well tolerated, furnishing isolated yields of 85%-91% to substituted NETHQ [Figure 4C]. Then, the substituents in 5-position were examined. The halide, methoxy, and 3-(1-piperidinyl) propoxy group are well tolerated, affording isolated yields of 84%-91% to substituted NETHQ. One of the products, the 6-[3-(1-piperidinyl) propoxy]-substituted NETHQ has been recognized as an effective H₃ receptor antagonist^[17,71]. It is noted that no clear effects of the position of the substituents on the yields to NETHQ are detected. Also, the isopropanol was applied as the substrate, affording 2-methyl THQ rather than the N-isopropyl-2-methyl THQ (isolated yield of 86%), as given in:



which implies the steric hindrance might suppress the N-alkylation of THQ.

Then the reaction is extended to the reaction of aliphatic 3-aminopropanol with ethanol. On Ni-NiAlZr-LDO [Figure 5A], the fraction of 3-aminopropanol decreases and that of 3-aminopropionaldehyde, pyridine, and piperidine increases firstly and then drops over time. Simultaneously, the fraction of N-ethyl piperidine increases over time [Figure 5A]. These results indicate that 3-aminopropanol first converts to 3-aminopropionaldehyde, which then undergoes cross-dual-condensation with acetaldehyde to form pyridine. Pyridine is hydrogenated to piperidine via hydrogen transfer, and finally, piperidine converts to N-ethyl piperidine through secondary cross-condensation [Supplementary Figure 23]. An isolated yield of 94% to N-ethyl piperidine has been afforded on Ni-NiAlZr-LDO in 48 h at 170 °C. However, on Ni-NiAl-LDO without Zr species, the reaction stops at piperidine and only traceable N-ethyl piperidine is detected in reaction of 3-aminopropanol with ethanol [Figure 5B]. A selectivity of 83% to piperidine is achieved on Ni-NiAl-LDO in 48 h at 170 °C. These results confirm that the introduction of Zr species promotes not only the dual-cross-condensation but also the secondary-cross-condensation. Interestingly, pyridine rather than 2,3-dihydropyridine is determined as a key intermediate for production of piperidine and then N-ethyl piperidine [Figure 5A and B].

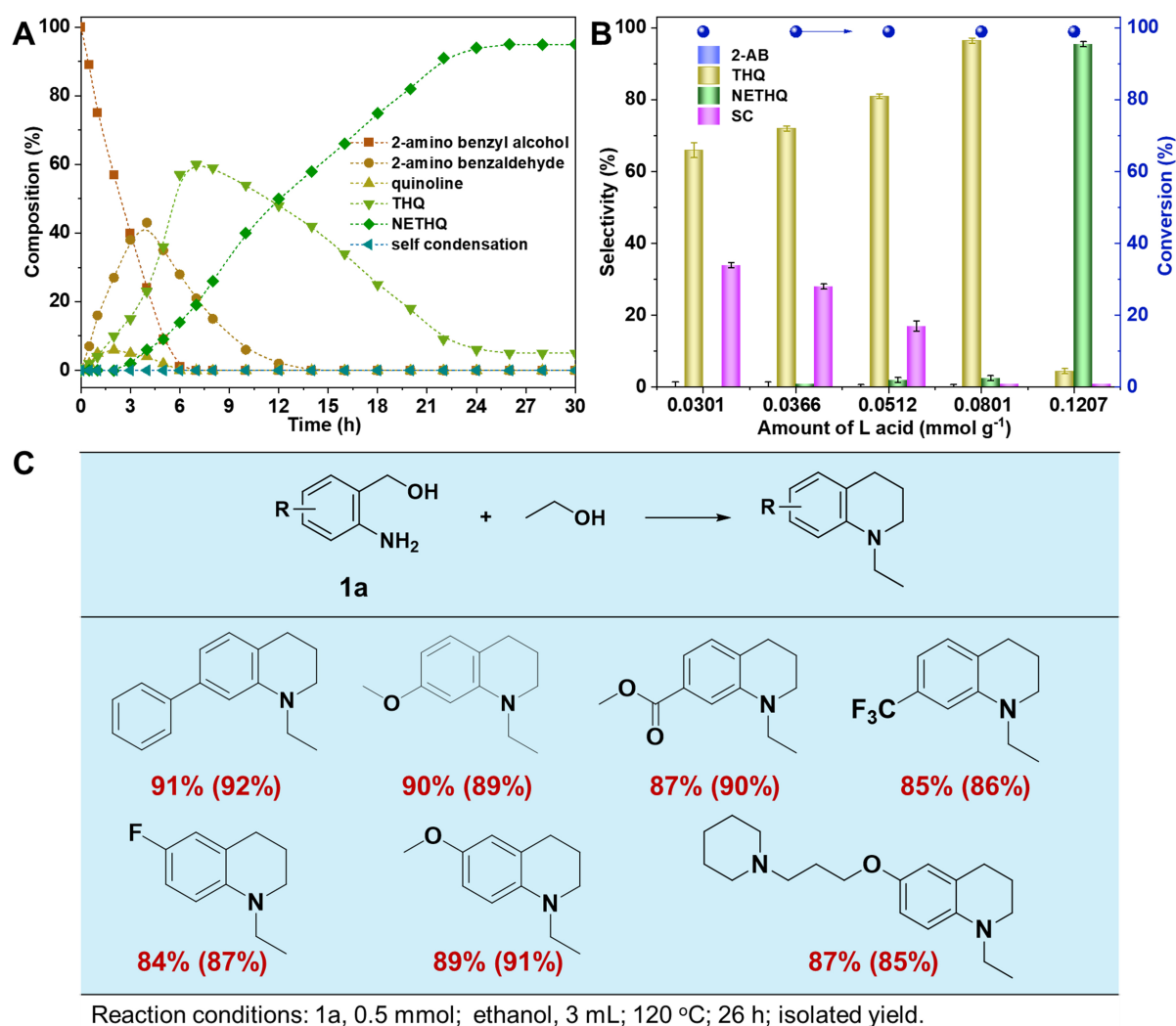


Figure 4. (A) Time course based on 2-aminobenzyl alcohol conversion in the reaction of 2-aminobenzyl alcohol with ethanol on Ni-NiAlZr-LDO at 120 °C under ambient atmosphere; (B) Catalytic performance on Ni-LDO in reaction of 2-aminobenzyl alcohol and ethanol at 120 °C in 26 h; (C) Substrates screening for Ni-NiAlZr-LDO catalyzed synthesis of NETHQ derivatives. The data in parentheses are reproduced results. LDO: Layered double oxides; NETHQ: N-ethyl-THQ; THQ: 1,2,3,4-tetrahydroquinoline.

Then the Ni-LDO was applied as catalyst in reaction of 2-aminoethanol with ethanol, the fraction of 2-aminoethanol declines while that of pyrrole, the dual-cross-condensation product from 2-aminoacetaldehyde and acetaldehyde, increases over time [Figure 5C]. A selectivity of 93% to pyrrole has been achieved in 24 h of reaction on Ni-NiAlZr-LDO. No 2-aminoacetaldehyde is detected during reaction, indicative of the rapid condensation between 2-aminoacetaldehyde and acetaldehyde. Similar results are detected on Ni-NiAl-LDO [Supplementary Figure 24], except for the pyrazine, the self-condensation product from 2-aminoacetaldehyde itself. Only a selectivity of 44% to pyrrole is obtained on Ni-NiAl-LDO [Supplementary Figure 24]. The selectivity to pyrrole almost linearly increases with increasing L acidic sites [Figure 5D], confirming that increasing the L acidic sites facilitates the dual-cross-condensation to form pyrrole. It is noted that the conjugation between the lone pair of electrons on N atom with C=C bond in pyrrole makes the hydrogenation of pyrrole proceed under 1 MPa of H₂ and hydrogen transfer is difficult to proceed [Supplementary Figure 25]. The reaction stops in pyrrole rather than tetrapyrrole in reaction of 2-aminoethanol with ethanol [Figure 5C and Supplementary Figure 24]. Also, the secondary alcohols are well

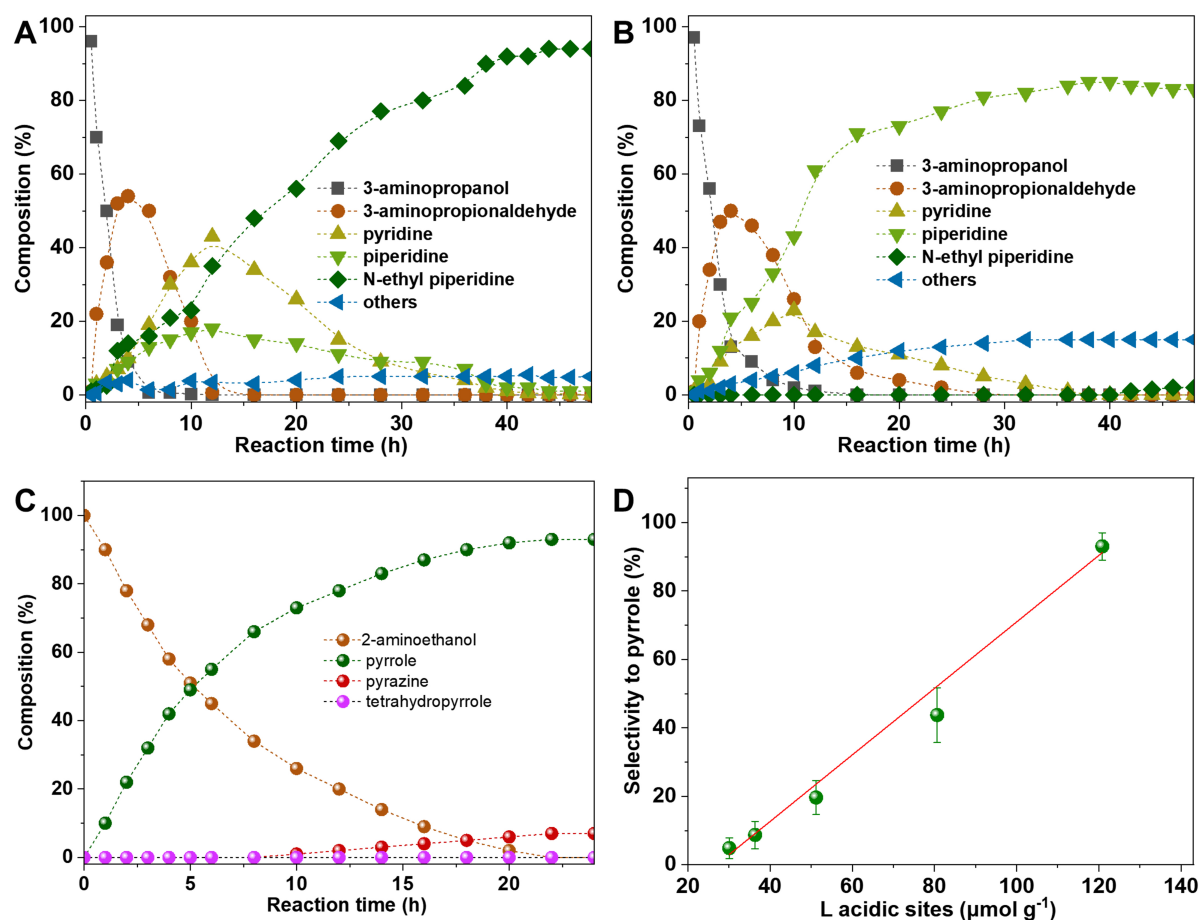


Figure 5. Time course based on 3-aminopropanol conversion in the reaction of 3-aminopropanol with ethanol at 170 °C under ambient atmosphere on Ni-NiAlZr-LDO (A) and Ni-NiAl-LDO (B); (C) Time course based on 2-aminoethanol conversion in the reaction of 2-aminoethanol with ethanol on Ni-NiAlZr-LDO at 120 °C under ambient atmosphere; (D) Correlation of the selectivity to dual-cross-condensation with L acidic sites in reaction of 2-aminoethanol with ethanol. LDO: Layered double oxides.

tolerated in the synthesis of pyrroles [Supplementary Table 3].

After 2 h in reaction of 2-aminoethanol with ethanol, the spent Ni-NiAlZr-LDO was simply recovered by centrifugation, thoroughly washed with ethanol. Then, the recovered Ni-NiAlZr-LDO was directly reused in the reaction of 2-aminoethanol with ethanol. Almost no decreases in either 2-aminoethanol conversion or pyrrole selectivity are observed in 25th run [Figure 6], showing excellent reusability and great potential for further industrialization.

Combined the above results with our previous reference, the catalytic cycle is illustrated [Figure 7]: (1) the ethanol and amino alcohol first convert to acetaldehyde and amino aldehyde via the dissociative adsorption of O–H bond on $\text{Ni}^{\delta+}$ and cleavage of $\alpha\text{--C--H}$ bond on Ni^0 to generate acetaldehyde bonded with support O; (2) the generated acetaldehyde and amino aldehyde dual-cross-condensate to form unsaturated N-containing heterocycles; (3) the hydrogenation of unsaturated N-containing heterocycles to saturated N-containing heterocycles rapidly occurs to form the saturated N-containing heterocycles by the active H species from the dehydrogenation step; (4) the strong L acidic sites facilitates the further activation of the saturated N-containing heterocycles to generate the N-ethyl N-containing heterocycles.

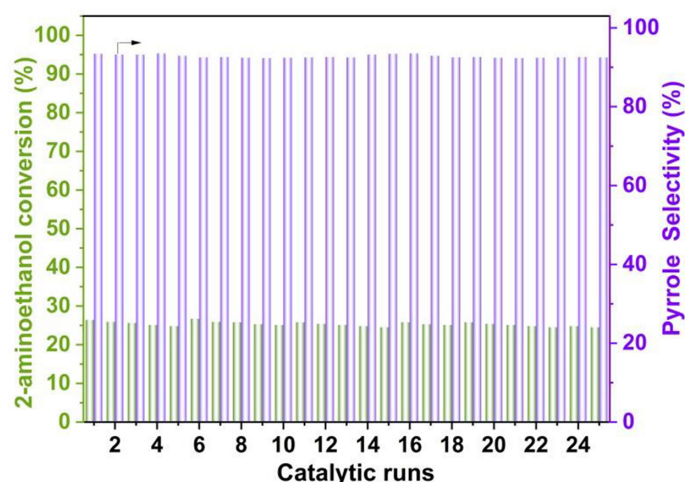


Figure 6. Reusability of Ni-NiAlZr-LDO in reaction of 2-aminoethanol and ethanol at 120 °C under ambient atmosphere. LDO: Layered double oxides.

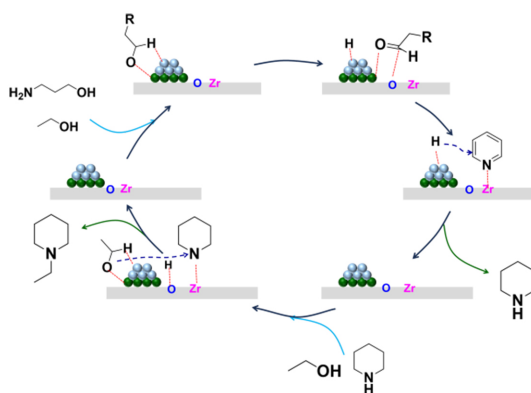


Figure 7. Proposed catalytic cycle for the synthesis of N-containing heterocycles from ethanol and amino alcohols on Ni-NiAlZr-LDO. LDO: Layered double oxides.

CONCLUSIONS

In conclusion, green and sustainable synthesis of N-containing heterocycles from bioethanol and amino alcohols has been achieved on Ni-LDO with tunable acidic sites via dehydrogenative dual-cross-condensation and even secondary-cross-condensation. Increasing acidic sites, especially strong L acidic sites, by Zr species not only promotes dual-cross-condensation but also provides strong adsorption sites of THQ/piperidine for the following secondary-cross-condensation of THQ to NETHQ and piperidine to N-ethyl piperidine. For the synthesis of five-membered N-containing heterocycles, the reaction stopped in pyrrole and the hydrogen transfer was suppressed. The mechanism for the modulation of hydrogen transfer for the synthesis of tetrapyrrole is also interesting and deserves to be investigated in detail.

DECLARATIONS

Authors' contributions

Conceptualized and supervised the project: An, Z.; He, J.

Synthesized the catalysts and performed the catalytic tests: Zhang, J.; Liang, L.

Performed the *in situ* FT-IR: Zhang, J.

Performed sample characterizations and data analysis: Zhang, J.

Reviewed the paper: Zhu, Y.; Shu, X.; Song, H.

All the authors discussed the results and revised the manuscript.

Availability of data and materials

The raw data supporting the findings of this study are available within this Article and its [Supplementary Materials](#). Further data is available from the corresponding authors upon reasonable request.

Financial support and sponsorship

This work was supported by the National Key R&D Program of China (2021YFB3801603) and National Natural Science Foundation of China (22138001 and 22288102).

Conflicts of interest

He, J. is Guest Editor of the Special Issue “She Energy-Catalysis for Sustainability: Advancements and Challenges” of the journal *Chemical Synthesis*. He, J. was not involved in any steps of editorial processing, notably including reviewer selection, manuscript handling, or decision-making. The other authors declare that there are no conflicts of interest.

Ethical approval and consent to participate

Not applicable.

Consent for publication

Not applicable.

Copyright

© The Author(s) 2025.

REFERENCES

1. Zhang, T. Taking on all of the biomass for conversion. *Science* **2020**, *367*, 1305-6. [DOI](#) [PubMed](#)
2. Feng, Y.; Long, S.; Tang, X.; et al. Earth-abundant 3d-transition-metal catalysts for lignocellulosic biomass conversion. *Chem. Soc. Rev.* **2021**, *50*, 6042-93. [DOI](#)
3. Li, G.; Wang, R.; Pang, J.; Wang, A.; Li, N.; Zhang, T. Production of renewable hydrocarbon biofuels with lignocellulose and its derivatives over heterogeneous catalysts. *Chem. Rev.* **2024**, *124*, 2889-954. [DOI](#)
4. Osman, A. I.; Nasr, M.; Aniagor, C. O.; et al. Synergistic technologies for a circular economy: upcycling waste plastics and biomass. *Front. Chem. Sci. Eng.* **2025**, *19*, 2507. [DOI](#)
5. Liu, C. G.; Xiao, Y.; Xia, X. X.; et al. Cellulosic ethanol production: Progress, challenges and strategies for solutions. *Biotechnol. Adv.* **2019**, *37*, 491-504. [DOI](#)
6. Zabed, H.; Sahu, J.; Boyce, A.; Faruq, G. Fuel ethanol production from lignocellulosic biomass: an overview on feedstocks and technological approaches. *Renew. Sust. Energ. Rev.* **2016**, *66*, 751-74. [DOI](#)
7. Manochio, C.; Andrade, B.; Rodriguez, R.; Moraes, B. Ethanol from biomass: a comparative overview. *Renew. Sust. Energ. Rev.* **2017**, *80*, 743-55. [DOI](#)
8. Yao, X.; Li, T.; Chung, S. H.; Ruiz-Martínez, J. Advances in the catalytic conversion of ethanol into nonoxygenated added-value chemicals. *Adv. Mater.* **2024**, *36*, e2406472. [DOI](#)
9. Zhang, J.; Yoo, E.; Davison, B. H.; et al. Towards cost-competitive middle distillate fuels from ethanol within a market-flexible biorefinery concept. *Green. Chem.* **2021**, *23*, 9534-48. [DOI](#)
10. Eagan, N. M.; Kumbhalkar, M. D.; Buchanan, J. S.; Dumesic, J. A.; Huber, G. W. Chemistries and processes for the conversion of ethanol into middle-distillate fuels. *Nat. Rev. Chem.* **2019**, *3*, 223-49. [DOI](#)
11. He, L.; Zhou, B.; Sun, D.; et al. Catalytic conversion of ethanol to oxygen-containing value-added chemicals. *ACS. Catal.* **2023**, *13*, 11291-304. [DOI](#)
12. Wang, J.; Qi, T.; Li, Z.; et al. A strategy of two-step tandem catalysis towards direct N-alkylation of nitroarenes with ethanol via facile fabricated novel Co-based catalysts derived from coordination polymers. *J. Catal.* **2019**, *376*, 106-18. [DOI](#)

13. Wang, J.; She, W.; Li, X.; et al. A highly efficient Co-based catalyst fabricated by coordination-assisted impregnation strategy towards tandem catalytic functionalization of nitroarenes with various alcohols. *J. Catal.* **2021**, *404*, 462-74. DOI
14. He, J.; Chen, L.; Liu, S.; Song, K.; Yang, S.; Riisager, A. Sustainable access to renewable N-containing chemicals from reductive amination of biomass-derived platform compounds. *Green. Chem.* **2020**, *22*, 6714-47. DOI
15. Xu, L.; Shi, C.; He, Z.; et al. Recent advances of producing biobased N-containing compounds via thermo-chemical conversion with ammonia process. *Energy. Fuels.* **2020**, *34*, 10441-58. DOI
16. Vitaku, E.; Smith, D. T.; Njardarson, J. T. Analysis of the structural diversity, substitution patterns, and frequency of nitrogen heterocycles among U.S. FDA approved pharmaceuticals. *J. Med. Chem.* **2014**, *57*, 10257-74. DOI PubMed
17. Sridharan, V.; Suryavanshi, P. A.; Menéndez, J. C. Advances in the chemistry of tetrahydroquinolines. *Chem. Rev.* **2011**, *111*, 7157-259. DOI PubMed
18. Muthukrishnan, I.; Sridharan, V.; Menéndez, J. C. Progress in the chemistry of tetrahydroquinolines. *Chem. Rev.* **2019**, *119*, 5057-191. DOI PubMed
19. Zhao, X.; Rudolph, M.; Asiri, A. M.; Hashmi, A. S. K. Easy access to pharmaceutically relevant heterocycles by catalytic reactions involving α -imino gold carbene intermediates. *Front. Chem. Sci. Eng.* **2020**, *14*, 317-49. DOI
20. Heo, Y. A.; Duggan, S. T. Niraparib: a review in ovarian cancer. *Target. Oncol.* **2018**, *13*, 533-9. DOI PubMed
21. Macchia, M.; Cervetto, L.; Demontis, G. C.; et al. New *N*-*n*-propyl-substituted 3-aryl- and 3-cyclohexylpiperidines as partial agonists at the D₄ dopamine receptor. *J. Med. Chem.* **2003**, *46*, 161-8. DOI
22. Shahane, S.; Louafi, F.; Moreau, J.; et al. Synthesis of alkaloids of *Galipea officinalis* by alkylation of an α -amino nitrile. *Eur. J. Org. Chem.* **2008**, *2008*, 4622-31. DOI
23. Shen, L.; Ye, Y. H.; Wang, X. T.; et al. Structure and total synthesis of aspernigerin: a novel cytotoxic endophyte metabolite. *Chemistry* **2006**, *12*, 4393-6. DOI
24. Chander, S.; Ashok, P.; Zheng, Y. T.; et al. Design, synthesis and *in-vitro* evaluation of novel tetrahydroquinoline carbamates as HIV-1 RT inhibitor and their antifungal activity. *Bioorg. Chem.* **2016**, *64*, 66-73. DOI
25. Ramnauth, J.; Renton, P.; Dove, P.; et al. 1,2,3,4-tetrahydroquinoline-based selective human neuronal nitric oxide synthase (nNOS) inhibitors: lead optimization studies resulting in the identification of *N*-(1-(2-(methylamino)ethyl)-1,2,3,4-tetrahydroquinolin-6-yl)thiophene-2-carboximidamide as a preclinical development candidate. *J. Med. Chem.* **2012**, *55*, 2882-93. DOI
26. Holsworth, D. D.; Jalaie, M.; Belliotti, T.; et al. Discovery of 6-ethyl-2,4-diaminopyrimidine-based small molecule renin inhibitors. *Bioorg. Med. Chem. Lett.* **2007**, *17*, 3575-80. DOI
27. Wang, X. F.; Wang, S. B.; Ohkoshi, E.; et al. *N*-aryl-6-methoxy-1,2,3,4-tetrahydroquinolines: a novel class of antitumor agents targeting the colchicine site on tubulin. *Eur. J. Med. Chem.* **2013**, *67*, 196-207. DOI PubMed PMC
28. Bai, L.; Sun, P.; Liu, Y.; et al. Novel aza-BODIPY based small molecular NIR-II fluorophores for *in vivo* imaging. *Chem. Commun.* **2019**, *55*, 10920-3. DOI
29. Boyarskiy, V. P.; Belov, V. N.; Medda, R.; Hein, B.; Bossi, M.; Hell, S. W. Photostable, amino reactive and water-soluble fluorescent labels based on sulfonated rhodamine with a rigidized xanthene fragment. *Chemistry* **2008**, *14*, 1784-92. DOI PubMed
30. Yamashita, K.; Imahashi, S.; Ito, S. Synthesis of benzylideneketone dyes and their photochemical properties as a sensitizer for alkali-developable photopolymerization systems. *Dyes. Pigments.* **2008**, *76*, 748-53. DOI
31. Tan, Z.; Liang, Y.; Yang, J.; Cao, L.; Jiang, H.; Zhang, M. Site-specific oxidative C–H chalcogenation of (hetero)aryl-fused cyclic amines enabled by nanocobalt oxides. *Org. Lett.* **2018**, *20*, 6554-8. DOI
32. Chen, X. W.; Zhao, H.; Chen, C. L.; Jiang, H. F.; Zhang, M. Hydrogen-transfer-mediated α -functionalization of 1,8-naphthyridines by a strategy overcoming the over-hydrogenation barrier. *Angew. Chem. Int. Ed. Engl.* **2017**, *56*, 14232-6. DOI
33. Zheng, D.; Yang, M.; Zhuo, J.; et al. Regio- and stereoselective benzylic hydroxylation to synthesize chiral tetrahydroquinolin-4-ol and tetrahydro-1H-benzo[b]jacepin-5-ol with *Pseudomonas plecoglossicidas*. *J. Mol. Catal. B-Enzym.* **2014**, *110*, 87-91. DOI
34. Chen, C.; Pan, Y.; Zhao, H.; et al. Ruthenium(II)-catalyzed regioselective C-8 hydroxylation of 1,2,3,4-tetrahydroquinolines. *Org. Lett.* **2018**, *20*, 6799-803. DOI
35. Zhao, H.; Zhao, S.; Li, X.; Deng, Y.; Jiang, H.; Zhang, M. Cobalt-catalyzed selective functionalization of aniline derivatives with hexafluoroisopropanol. *Org. Lett.* **2019**, *21*, 218-22. DOI
36. Yi, C. S.; Yun, S. Y.; Guzei, I. A. Catalytic synthesis of tricyclic quinoline derivatives from the regioselective hydroamination and C–H bond activation reaction of benzocyclic amines and alkynes. *J. Am. Chem. Soc.* **2005**, *127*, 5782-3. DOI PubMed
37. Jia, Y. X.; Kündig, E. P. Oxindole synthesis by direct coupling of C(sp²)-H and C(sp³)-H centers. *Angew. Chem. Int. Ed. Engl.* **2009**, *48*, 1636-9. DOI
38. Lan, L.; Li, Y.; Zhu, J.; et al. Highly flexible polypyrrole electrode with acanthosphere-like structures for energy storage and actuator applications. *Chem. Eng. J.* **2023**, *455*, 140675. DOI
39. Lohani, P. C.; Tiwari, A. P.; Chhetri, K.; et al. Polypyrrole nanotunnels with luminal and abluminal layered double hydroxide nanosheets grown on a carbon cloth for energy storage applications. *ACS. Appl. Mater. Interfaces.* **2022**, 23285-96. DOI
40. Wang, S.; Chen, Y.; Hu, B.; Wang, Y.; Jing, X.; Li, Y. Polypyrrole micro/nanostructures and their soft materials in versatile forms: construction and applications. *Mater. Chem. Front.* **2024**, *8*, 434-54. DOI
41. Jain, R.; Jadon, N.; Pawaiya, A. Polypyrrole based next generation electrochemical sensors and biosensors: a review. *TrAC-Trend. Anal. Chem.* **2017**, *97*, 363-73. DOI
42. Wang, W.; Lv, Y.; Liu, H.; Cao, Z. Recent advances in application of polypyrrole nanomaterial in water pollution control. *Sep. Purif.*

- Technol. 2024, 330, 125265. DOI
43. Knorr, L. Einwirkung des Diacetbernsteinsäureesters auf Ammoniak und primäre Aminbasen. *Ber. Dtsch. Chem. Ges.* **1885**, 18, 299-311. (in German). DOI
 44. Paal, C. Synthese von Thiophen- und Pyrrolderivaten. *Ber. Dtsch. Chem. Ges.* **1885**, 18, 367-71. (in German). DOI
 45. The Goodyear Tire & Rubber Company. Hydrogenation of heterocyclic compounds. GB395231A, 1933.
 46. Hewitt, J. H.; West, T. F. Process for the preparation of compounds containing fused pyridine rings. US2358162A, 1944.
 47. Lafon, L. 2,4,6-Trimethoxyphenyl 3-(1,2,3,4-tetrahydro-1-quinoliny)propyl ketone, useful as sedative. FR2534914, 1984.
 48. Biller, S. A.; Misra, R. N. 1,2,3,4-tetrahydro-8-quinolinol derivatives and anti-allergic use thereof. US4843082A, 1989.
 49. Michlik, S.; Kempe, R. A sustainable catalytic pyrrole synthesis. *Nat. Chem.* **2013**, 5, 140-4. DOI
 50. Srimani, D.; Ben-David, Y.; Milstein, D. Direct synthesis of pyrroles by dehydrogenative coupling of β -aminoalcohols with secondary alcohols catalyzed by ruthenium pincer complexes. *Angew. Chem. Int. Ed. Engl.* **2013**, 52, 4012-5. DOI PubMed
 51. Kallmeier, F.; Dudziec, B.; Irrgang, T.; Kempe, R. Manganese-catalyzed sustainable synthesis of pyrroles from alcohols and amino alcohols. *Angew. Chem. Int. Ed. Engl.* **2017**, 56, 7261-5. DOI PubMed
 52. Pan, B.; Liu, B.; Yue, E.; et al. A ruthenium catalyst with unprecedented effectiveness for the coupling cyclization of γ -amino alcohols and secondary alcohols. *ACS. Catal.* **2016**, 6, 1247-53. DOI
 53. Michlik, S.; Kempe, R. Regioselectively functionalized pyridines from sustainable resources. *Angew. Chem. Int. Ed. Engl.* **2013**, 52, 6326-9. DOI PubMed
 54. Hille, T.; Irrgang, T.; Kempe, R. Synthesis of meta-functionalized pyridines by selective dehydrogenative heterocondensation of β - and γ -amino alcohols. *Angew. Chem. Int. Ed. Engl.* **2017**, 56, 371-4. DOI PubMed
 55. Wang, B.; Li, M.; Zhang, S.; Wu, H.; Liao, Y.; Li, H. Synergistic effect between Co single atoms and nanoparticles enables selective synthesis of bio-based benzimidazoles. *Appl. Catal. B-Environ.* **2023**, 327, 122454. DOI
 56. Mastalir, M.; Glatz, M.; Pittenauer, E.; Allmaier, G.; Kirchner, K. Sustainable synthesis of quinolines and pyrimidines catalyzed by manganese PNP pincer complexes. *J. Am. Chem. Soc.* **2016**, 138, 15543-6. DOI PubMed
 57. Forberg, D.; Schwob, T.; Kempe, R. Catalytic condensation for the formation of polycyclic heteroaromatic compounds. *Nat. Commun.* **2018**, 9, 1751. DOI PubMed PMC
 58. Shee, S.; Ganguli, K.; Jana, K.; Kundu, S. Cobalt complex catalyzed atom-economical synthesis of quinoxaline, quinoline and 2-alkylaminoquinoline derivatives. *Chem. Commun.* **2018**, 54, 6883-6. DOI PubMed
 59. Chakraborty, S.; Piszcz, P. E.; Hayes, C. E.; Baker, R. T.; Jones, W. D. Highly selective formation of n-butanol from ethanol through the Guerbet process: a tandem catalytic approach. *J. Am. Chem. Soc.* **2015**, 137, 14264-7. DOI PubMed
 60. Zhang, J.; An, Z.; Zhu, Y.; et al. $\text{Ni}^0/\text{Ni}^{\delta+}$ synergistic catalysis on a nanosized Ni surface for simultaneous formation of C-C and C-N bonds. *ACS. Catal.* **2019**, 9, 11438-46. DOI
 61. Zhao, Y.; Li, F.; Zhang, R.; Evans, D. G.; Duan, X. Preparation of layered double-hydroxide nanomaterials with a uniform crystallite size using a new method involving separate nucleation and aging steps. *Chem. Mater.* **2002**, 14, 4286-91. DOI
 62. Grosvenor, A. P.; Biesinger, M. C.; Smart, R. S.; McIntyre, N. S. New interpretations of XPS spectra of nickel metal and oxides. *Surf. Sci.* **2006**, 600, 1771-9. DOI
 63. Das, S.; Thakur, S.; Bag, A.; Gupta, M. S.; Mondal, P.; Bordoloi, A. Support interaction of Ni nanocluster based catalysts applied in CO_2 reforming. *J. Catal.* **2015**, 330, 46-60. DOI
 64. Chen, W.; Chan, A.; Sun-waterhouse, D.; Moriga, T.; Idriss, H.; Waterhouse, G. I. Ni/TiO_2 : a promising low-cost photocatalytic system for solar H_2 production from ethanol-water mixtures. *J. Catal.* **2015**, 326, 43-53. DOI
 65. Ma, G.; Liu, D.; Allen, H. C. Piperidine adsorption on hydrated alpha-alumina (0001) surface studied by vibrational sum frequency generation spectroscopy. *Langmuir* **2004**, 20, 11620-9. DOI PubMed
 66. Zhao, J.; Chen, H.; Xu, J.; Shen, J. Effect of surface acidic and basic properties of the supported nickel catalysts on the hydrogenation of pyridine to piperidine. *J. Phys. Chem. C.* **2013**, 117, 10573-80. DOI
 67. Aarts, J.; Sassen, N. Piperidine adsorbed on Pd(111) studied by electron energy loss spectroscopy. *Surf. Sci.* **1990**, 225, 35-9. DOI
 68. Ochoa, J. V.; Trevisanut, C.; Millet, J. M.; Busca, G.; Cavani, F. *In Situ* DRIFTS-MS study of the anaerobic oxidation of ethanol over spinel mixed oxides. *J. Phys. Chem. C.* **2013**, 117, 23908-18. DOI
 69. Zhang, Z.; Wang, Y.; Lu, J.; et al. Pr-doped CeO_2 catalyst in the prins condensation-hydrolysis reaction: are all of the defect sites catalytically active? *ACS. Catal.* **2018**, 8, 2635-44. DOI
 70. Rousseau, S.; Marie, O.; Bazin, P.; Daturi, M.; Verdier, S.; Harlé, V. Investigation of methanol oxidation over Au/catalysts using operando IR spectroscopy: determination of the active sites, intermediate/spectator species, and reaction mechanism. *J. Am. Chem. Soc.* **2010**, 132, 10832-41. DOI PubMed
 71. Jesudason, C. D.; Beavers, L. S.; Cramer, J. W.; et al. Synthesis and SAR of novel histamine H_3 receptor antagonists. *Bioorg. Med. Chem. Lett.* **2006**, 16, 3415-8. DOI